Journal of Structural Geology 63 (2014) 50–67

Contents lists available at ScienceDirect

Journal of Structural Geology

journal homepage: www.elsevier.com/locate/jsg

Anisotropy of permeability in faulted porous sandstones

N.J.C. Farrell*, D. Healy, C.W. Taylor

School of Geosciences, King's College, University of Aberdeen, Aberdeen AB24 3UE, United Kingdom

ARTICLE INFO

Article history:
Received 31 October 2013
Received in revised form
12 February 2014
Accepted 22 February 2014
Available online 3 March 2014

Keywords:
Permeability
Anisotropy
Faulting
Porous sandstone
Cataclasis
Confining pressure

ABSTRACT

Studies of fault rock permeabilities advance the understanding of fluid migration patterns around faults and contribute to predictions of fault stability. In this study a new model is proposed combining brittle deformation structures formed during faulting, with fluid flow through pores. It assesses the impact of faulting on the permeability anisotropy of porous sandstone, hypothesising that the formation of fault related micro-scale deformation structures will alter the host rock porosity organisation and create new permeability pathways. Core plugs and thin sections were sampled around a normal fault and oriented with respect to the fault plane. Anisotropy of permeability was determined in three orientations to the fault plane at ambient and confining pressures. Results show that permeabilities measured parallel to fault dip were up to 10 times higher than along fault strike permeability. Analysis of corresponding thin sections shows elongate pores oriented at a low angle to the maximum principal palaeo-stress (σ_1) and parallel to fault dip, indicating that permeability anisotropy is produced by grain scale deformation mechanisms associated with faulting. Using a soil mechanics 'void cell model' this study shows how elongate pores could be produced in faulted porous sandstone by compaction and reorganisation of grains through shearing and cataclasis.

Introduction

Fluid flow around faults is controlled by geometrically complex structures at a variety of scales. Studies aimed at quantifying the geometry of these fault generated micro-structures in relation to fault induced permeability anisotropy have been carried out in low porosity protolith fault rocks (Faulkner and Rutter, 1998; Evans et al., 1997; Wibberley and Shimamoto, 2005; Cavailhes et al., 2013). However, determining the contribution of fault generated porosity to permeability anisotropy in sandstones with pre-existing high porosities, i.e. those more typical of water and hydrocarbon reservoir rocks, has not been attempted on natural examples. Faults are complex features of deformation that are often divided into two main units: fault core and fault damage zone (Chester and Logan, 1986). Each unit contains characteristic micro-scale deformation structures that can determine the linked pore space to create new localised connective conduits (Caine et al., 1996). Models of fluid flow around faults are often simplified for a reservoir scale and do not account for localised, small scale permeability heterogeneities and anisotropies formed by these micro-scale deformation structures. However, the importance of accurately up-scaling any micro-scale heterogeneities and anisotropies identified by high resolution field based data has been established through testing flow simulation models assessed with and without these features (Flodin et al., 2001). Results from this study show that identifying small scale, discrete permeability pathways may actually reveal common deformation derived permeability patterns, which could contribute to bulk fault-permeability anisotropy (Flodin et al., 2001). Investigation of preferential permeability pathways and an improved understanding of the geometries of pore structures controlling them are important for fault seal analysis in the petroleum and carbon storage industries, as well as contributing to predictions of pore fluid pressure and fault stability in reservoirs and top seals (Healy, 2012). These analyses are vital for the extraction of oil and gas during production as water injection is commonly used to maintain pressures in depleted reservoirs and to enhance recovery efficiency.

Previous studies using core plug permeabilities have shown that fault rocks can have a significant degree of permeability anisotropy (Faulkner and Rutter, 1998; Evans et al., 1997; Shipton et al., 2002; Wibberley and Shimamoto, 2005; Cavailhes et al., 2013). Studies by Faulkner and Rutter (1998), Evans et al. (1997), Wibberley and Shimamoto (2005) and Cavailhes et al. (2013) measured the permeability of core plugs oriented orthogonal to the fault plane. The orientations of microstructures observed in thin sections can

* Corresponding author. Geology Department, School of Geosciences, University of Aberdeen, Meston Building, Aberdeen AB24 3UE, United Kingdom.
E-mail addresses: n.farrell@abdn.ac.uk, natterslive@msn.com (N.J.C. Farrell).

http://dx.doi.org/10.1016/j.jsg.2014.02.008

then be put into the context of the principal stresses active during faulting allowing comparison of patterns of pore connectivity between studies. These studies concentrate on faults in low porosity (<5%) host rocks including graphitic mica schist, crystalline granite and deeply buried arkosic sandstones respectively. For the assessment of permeability anisotropy in more common reservoir rocks we need to study samples from faulted porous sandstones.

Anisotropic permeability

A rock is considered to show anisotropy of permeability when the measured permeability varies depending on the direction of fluid flow through the sample (Meyer, 2002). Permeability anisotropy can be produced through the formation of oriented fabrics and foliations during deposition and deformation or through the preferential orientation of pore connectivity (including porosity from open microfractures) during deformation.

Undeformed host rock permeability anisotropy is documented in a range of sandstone facies and is attributed to preferential fluid pathways produced by grain scale porosity heterogeneities formed by depositional sedimentary fabrics such as lamination (Lewis et al., 1988). Permeabilities measured on core plugs oriented parallel to, and normal to, aeolian laminations in dune facies of the host rock used in this study, show that maximum permeability occurs parallel to the depositional lamination. This is due to well sorted grains with good lateral continuity of pores. Minimum permeability is perpendicular to the laminations due to a more variable grain size distribution plus compaction and pore collapse during burial.

Changes in porosity due to deformation are controlled by alterations in grain size and grain size distributions and by the production of microstructures which can modify pore connectivity. Increases in porosity can occur through formation of microfractures and dilatancy associated with cataclasis. Secondary porosity can also be formed through dissolution of grains associated with increased fluid flow. Decreases in porosity can occur due to grain size rearrangement (pore collapse), reduction (cataclasis) and cementation. This study aims to assess the impact of normal faulting on the permeability anisotropy of porous aeolian sandstone, hypothesising that the formation of fault related micro-scale deformation structures will alter the host rock depositional porosity organisation and create new permeability pathways measurable on core scale samples.

Permeability anisotropy in laboratory samples

Experimental studies on deformed rocks have identified permeability anisotropy (Zoback and Byerlee, 1976; Zhu et al., 2002). In both of these studies tests were conducted on core plugs of porous sandstone deformed in two structural regimes; uniaxial extension and uniaxial compression, simulating permeabilities oriented parallel and normal to the maximum principal stress. The first of these deformation experiments conducted on unconsolidated porous sandstone plugs confined at high pressures demonstrates permeability anisotropy in two orientations with permeability maximum normal to the direction of maximum compression (or maximum principal stress) (Zoback and Byerlee, 1976). Thin sections made from samples after compression revealed significant grain breakage in samples taken to high confining pressures (>75 MPa), which may have influenced the permeability anisotropy observed. In contrast experimental results from a later study on consolidated (cemented) sandstone core plugs show that permeabilities parallel to the direction of maximum principal stress are generally higher than in the direction of minimum principal stress (Zhu et al., 2002). Analyses of experimental test results suggest a link between permeability anisotropy and grain scale patterns, inferring a connection between deformation textures and permeability anisotropy. Interpretation of consolidated sandstone experiments concludes that preferential flow pathways parallel to the maximum stress direction are caused by preferential alignment of microcracks parallel to the maximum stress orientation (Zhu et al., 2002). The variation between the directions of maximum permeability between these two experimental studies is probably due to the variability between consolidation states of samples. Permeability anisotropy produced by deformation texture is also observed in an experimental study involving shearing artificial quartz gouge (Zhang and Tullis, 1998). In this study permeability anisotropy of one order of magnitude is identified, with maximum permeability parallel to the fault plane and at a low angle to the maximum stress direction. Minimum permeability is perpendicular to the fault plane. Results from this study also suggest that the magnitude of permeability anisotropy is dependent on the degree of shear localisation as this enhances the permeability contrast between localised zones and the rest of the fault (Zhang and Tullis, 1998).

The results of experimental tests are not directly comparable with the permeability structure around a natural fault. Permeability measurements collected from the same core while in extension and then compression (Zoback and Byerlee, 1976; Zhu et al., 2002) are not being conducted at the same time under the same stress conditions; therefore they are unlikely to be measuring fluid flow through the same fixed pore network. An additional limitation of these experimental tests is that permeability measurements can only be taken in two orientations to the maximum principal stress rather than three orientations, neglecting the impact of fault kinematics on the orientation and geometry of deformation structures formed and the resulting permeability anisotropy. Results from existing studies of cores collected from natural faults measuring permeability anisotropy in three separate orientations to the fault plane are described in the following section.

Permeability anisotropy around faults

Direct quantitative studies of permeability anisotropy (using confined/closed system permeability tests) on oriented core plugs taken from natural faults in any lithology are uncommon (Evans et al., 1997; Faulkner and Rutter, 1998; Shipton et al., 2002; Wibberley and Shimamoto, 2005; Cavailhes et al., 2013; Saillet and Wibberley, 2013). These studies depict permeability in three different structural settings and three lithologies. In a study of permeability structure around a normal fault in aeolian sandstone host rock, two samples of deformed aeolian sandstone were cored in three orientations and showed permeability anisotropy in two directions (Shipton et al., 2002). Minimum permeabilities were identified in cores that are cross cut by localised deformation bands, highlighting the importance of fault architecture components comprising of meso-scale, localised features like deformation bands on influencing permeability anisotropy in porous aeolian sandstones. These cores were not oriented with respect to a main fault plane and principal stresses and therefore the role of fault kinematics in creating permeability anisotropies cannot be studied. A detailed study of permeability anisotropy in relation to faulting is presented in an investigation of thrust faulting in crystalline granites (Evans et al., 1997). This study used samples cored in three orientations, one orthogonal to the fault plane. Analysis of permeability measurements from 31 core plugs concluded that maximum permeability is oriented parallel to the fault plane and parallel to the slip direction (down fault dip), intermediate permeability is parallel to the fault plane and perpendicular to the fault slip and minimum permeability is perpendicular to the fault

plane. A further field-based study using cores plugged in three orientations to the strike-slip Carboneras Fault shows anisotropy of permeability in the clay bearing fault gouge formed from graphitic mica schist protolith (Faulkner and Rutter, 1998). Results from six core plugs showed that permeability was higher normal to fault transport direction than along fault strike and minimum permeabilities were normal to the fault plane. Maximum permeability parallel to the fault but perpendicular to fault transport direction is also recorded in clay-rich, slip zone gouge samples collected from the strike-slip, Median Tectonic Line in Japan (Wibberley and Shimamoto, 2005). A more recent study that measured the permeability of foliated arkosic sandstones in three orientations around two normal faults in the Grés d'Annot identified anisotropy of permeability in two directions with maximum permeability oriented along fault strike, perpendicular to the shear displacement (Cavailhes et al., 2013).

These studies all link preferential fluid flow pathways to fault rock microstructure, concluding that permeability anisotropy is controlled by microstructures and/or fabrics developed during faulting. The main control on permeability identified in each study varies depending on the composition of the original protolith. In crystalline granites, enhanced porosity formed by fracturing and cataclasis is identified as the dominant control on permeability anisotropy (Evans et al., 1997). In low porosity, phyllosilicate rich fault rocks of the Carboneras Fault (Faulkner and Rutter, 1998), the Median Tectonic Line (Wibberley and Shimamoto, 2005) and the Grés d'Annot faults (Cavailhes et al., 2013), anisotropic foliations interacting with shear structures and veining are recognised as the main influence on permeability anisotropy.

Samples in this study were collected from a normal fault in aeolian dune facies, porous sandstone protolith. In contrast to protoliths of graphitic mica schist, low porosity, arkosic sandstone or crystalline granite, porous aeolian sandstones have a pre-existing porosity of >20% that is made up of pore network arrangements formed during deposition which produce pre-existing permeability anisotropy. Unlike the phyllosilicate rich protolith of the Carboneras fault and Median Tectonic Line or the arkosic, phyllosilicate rich sandstone of the Grés D'Annot, aeolian sandstones do not have any significant clay content to form anisotropic foliations during deformation. However, the quartz grains in deformed sandstones are commonly cataclased, altering grain size and grain distribution thereby transforming the depositional porosity to construct a new pore network. Following the methodology of previous studies, this deformation-related porosity may be recognised as anisotropy in permeability that can be measured relative to the normal fault plane. Assuming the orientation of principal stresses and subsequent fault kinematics influences the development of permeability anisotropy, the permeability anisotropy around a normal fault may be characterised by three principal directions. As the maximum permeability orientation for a strike-slip fault is normal to the direction of transport (Faulkner and Rutter, 1998; Wibberley and Shimamoto, 2005), maximum permeability around a normal fault may be hypothesised to be oriented along fault strike, as observed in normal faults in the Grés d'Annot (Cavailhes et al., 2013). In contrast, maximum permeability in a thrust fault study is in the direction of transport (Evans et al., 1997) therefore maximum permeability around a normal fault should be inferred to be parallel to fault dip.

In this study, permeabilities of oriented core plugs from 12 cataclasite samples collected around a normal fault were measured at ambient and reservoir simulating confining pressures (10–100 MPa). Core orientations relative to the fault plane were; normal to the fault (x), along fault strike (y) and parallel to fault dip (z). The results are interpreted in the context of permeability anisotropy around a normal fault in porous sandstone as a product of microstructures produced during extensional faulting. It also examines how these preferential flow pathways could impact on the distribution of fluids around a normal fault. Lastly, we assess the potential significance of an improved understanding of permeability anisotropy and its evolution during faulting.

Geological background and sample locations

The North Sea has two main areas of subsidence associated with Permo-Triassic tectonics named the northern and southern Permian basins (Glennie, 1983), which contain some of the North Sea's most viable hydrocarbon reservoirs. Another small Permian basin is located in the Moray Firth. This north-east to south-west trending basin is defined by a number of reactivated extensional faults including the Helmsdale Fault system to the north-west and the Lossiemouth Fault system to the south, and partially by the Wick Fault system in the north (Underhill, 1991). Faults in the Lossiemouth Fault system are exposed onshore and are accessible at localities along the coast of Moray between Burghead and Lossiemouth. Outcrops are mainly composed of Permo-Triassic Hopeman Sandstone Formation (Benton and Walker, 1985). The Hopeman Sandstone is a well sorted, fine to medium grained, quartz rich, quartz cemented sandstone deposited in an aeolian setting (Shotton, 1956; Peacock et al., 1968; Glennie and Buller, 1983; Edwards et al., 1993; Quinn unpublished thesis, 2005) similar to sandstones comprising the Rotliegend gas reservoirs in the southern North Sea (Hinai et al., 2008). The study area presents an opportunity to address the influence of normal faulting on porous sandstones in a relatively homogenous rock with a direct hydrocarbon field analogue.

The Clashach Fault is a seismic scale normal fault with the Hopeman Sandstone Formation in both the hanging wall and footwall (Edwards et al., 1993; Prieto, 2010). Fault throw is estimated at a maximum of 50 m (Quinn, unpublished thesis, 2005) calculated from borehole measured onshore thickness of Hopeman Sandstone Formation of 60 m (Berridge and Ivimey-Cook, 1967). The fault is very well exposed in Clashach Cove and the fault core can be traced laterally for over 1 km from east to west (Fig. 1). Along these exposures the main fault can be observed as a well-developed core 50–100 cm wide in Clashach Cove, with narrower fault core evident at localities either side of the cove to the west and east where the fault may be 'tipping' out. Alternatively these outcrops could constitute fault splays or segments of the main fault. Kinematic indicators include slickenlines plunging between 70° and 83°W, indicating a slightly oblique but predominantly normal dip-slip shear sense.

Auxiliary field data was collected to contextualise samples in a framework of qualitative and quantitative changes in the sedimentology and structure. Field data collected includes the orientations of tectonic features and descriptions of structural styles, and sedimentary analysis of centimetre scale logs at six locations.

Oriented samples were collected from three localities with good exposure of the fault core, hanging wall and footwall: Clashach quarry, Clashach Cove east and Clashach Cove west (Fig. 1). A few samples were collected from a fourth locality comprising a well exposed fault core and footwall exposure representing a possible splay fault off the main Clashach fault, termed 'The Golf course fault'. Detailed maps and cross sections through the Clashach fault zone show that fault architecture varies between these localities. Fault core exposures at all localities are composed of variable thickness fault breccias (10–100 cm), units of pervasively cataclased fault rock with multiple polished slip surfaces and a composite unit of anastamosing deformation bands (Fig. 2).

At each locality a number of different fracture types are visible including, high and low angle joints, iron stained fractures and individual and composite cataclastic deformation bands, at varying

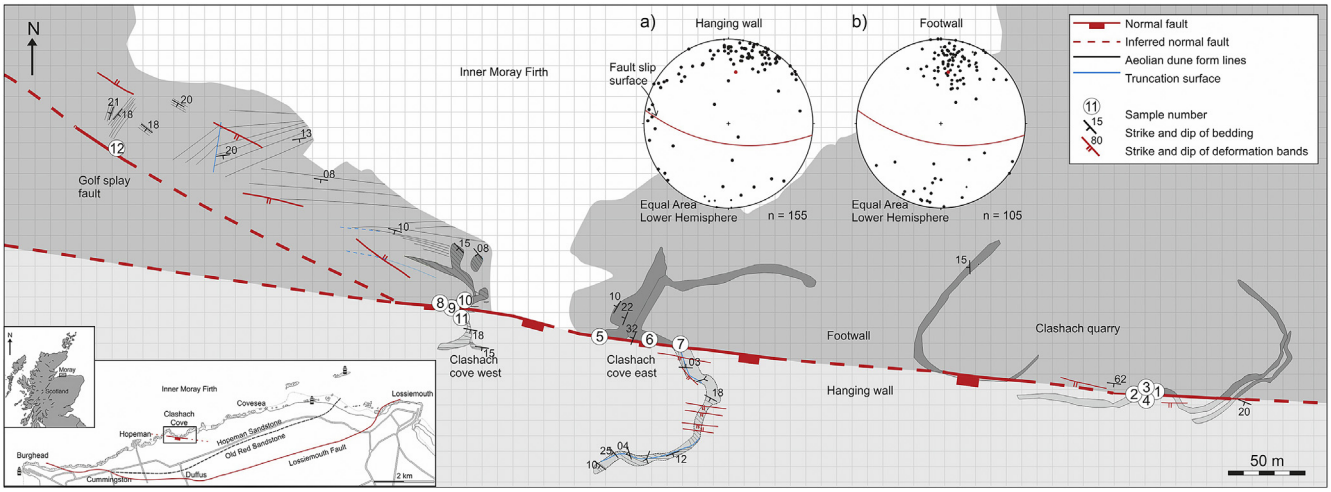

Fig. 1. Geological map showing the location of the Clashach Fault in Clashach Cove, Moray, Scotland. A geological sketch map in the bottom left shows Hopeman Sandstone Formation juxtaposed against Old Red Sandstone (after Peacock et al., 1968). The fault footwall is marked in a darker shade of grey than the hanging wall and outcrops are outlined and depicted by a darker tone. Stereonets show poles to deformation bands from the hanging wall and footwall. Sample locations are numbered 1 to 12.

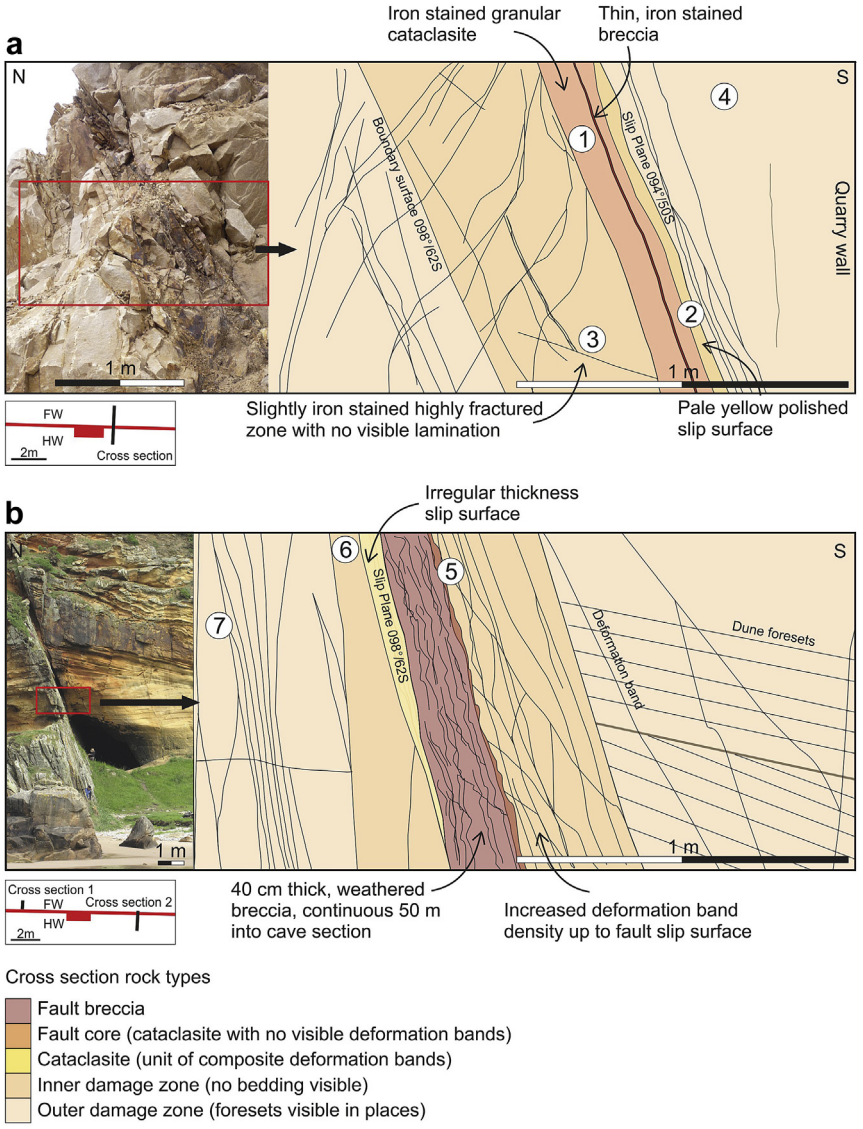

Fig. 2. Cross sections showing the fault architecture at a) Clashach Quarry and b) Clashach Cove East. Cross section locations are marked on photographs and sketch maps below (section b is made from two amalgamated sections due to access). Sample locations are marked in white circles.

spatial intensities extending up to 50 m either side of the main fault slip face. Fracture intensities were measured using the circular scanline method (Mauldon et al., 1999), with scan lines oriented perpendicular to the fault plane in the hanging wall and footwall. Although all fractures were measured, only deformation band intensities are displayed here as they are considered to be contemporaneous with faulting (Fig. 3). Deformation band intensities are high (15–20 m^{-1}) within the first 3 m of the damage zone in both hanging wall and footwall and decreasing (2–5 m^{-1}) away from the fault plane. Fracture intensities are higher in the footwall than the hanging wall. Along fault strike deformation bands are relatively discontinuous (<5 m length) and anastamosing. In contrast, in cross section deformation bands are very continuous (>20 m) and straight.

Twelve 20 × 20 cm oriented samples of relatively homogeneous cataclastic fault rock were collected to examine the heterogeneity of petrophysical properties around the fault (Fig. 1). Samples were collected where sedimentary lamination is no longer visible due to pervasive, distributed cataclasis, within 50 cm of the fault plane (Fig. 2). Samples containing localised cataclastic deformation bands were avoided. All samples (excluding Sample 12) were collected from aeolian dune facies so had comparable original grain sizes and associated host rock petrophysical properties. This was checked by tracing sampled units away from the fault plane the locations of sedimentary logs where original facies could be assessed.

Laboratory methods

Equipment

Single phase permeability was measured along the axial direction of core plugs using nitrogen (N_2) gas as the pore fluid in a permeameter with a Hassler sleeve pressurised to 400 psi to avoid gas leakage around the sides of the core. To investigate properties at subsurface conditions, core plug permeability was also measured in a confining pressure permeameter again using N_2 gas as pore fluid. Core plug porosity was measured using a helium injection method in a porosimeter.

Samples

A total of 45 core plugs 2.54 cm in diameter and of varying lengths between 2.54 and 5.08 cm were made from the 12 field sample blocks of cataclased sandstone. Each block was cored in three orientations: normal to the fault (x), along fault strike (y) and parallel to fault dip (z) (Fig. 4). Nine of the 45 samples constitute multiple samples in a single direction. In addition, 11 further cores were plugged in a single direction from two fault rock samples to assess the heterogeneity of permeability. A total of 36 thin sections corresponding to each of the oriented core plugs were prepared for digital image analysis. Thin sections were injected with blue epoxy resin to highlight pore space.

An appraisal of core quality was made to identify chipped or disfigured cores and detect any notable structural features, e.g. deformation bands, which may affect the permeability. Before measurement, all samples were washed and then dried for 24 h in an oven at 40 °C to eliminate pore water.

The permeability of undeformed host rock samples was also measured in the framework of core plugs oriented in three orientations, one orthogonal to the fault plane using field orientation relationships of lamination to the fault plane mapped at Clashach cove (Fig. 1). Results from 24 undeformed host rock cores taken from three samples show maximum permeability in two directions, normal to the fault plane (x) and along fault strike (y). Both x and y core orientations are sub-parallel to sedimentary laminations. Minimum permeabilities are shown in cores oriented parallel to fault dip (z) and sub-perpendicular to sedimentary lamination (Fig. 5).

Methods

Steady state permeabilities from 45 cores were measured using a permeameter at ambient pressures. Tests were run at room temperatures, 18–20 °C. Ambient pressure permeability is calculated using a modified Darcy equation – which normalises changes in pressure by mean pressure – expressed as,

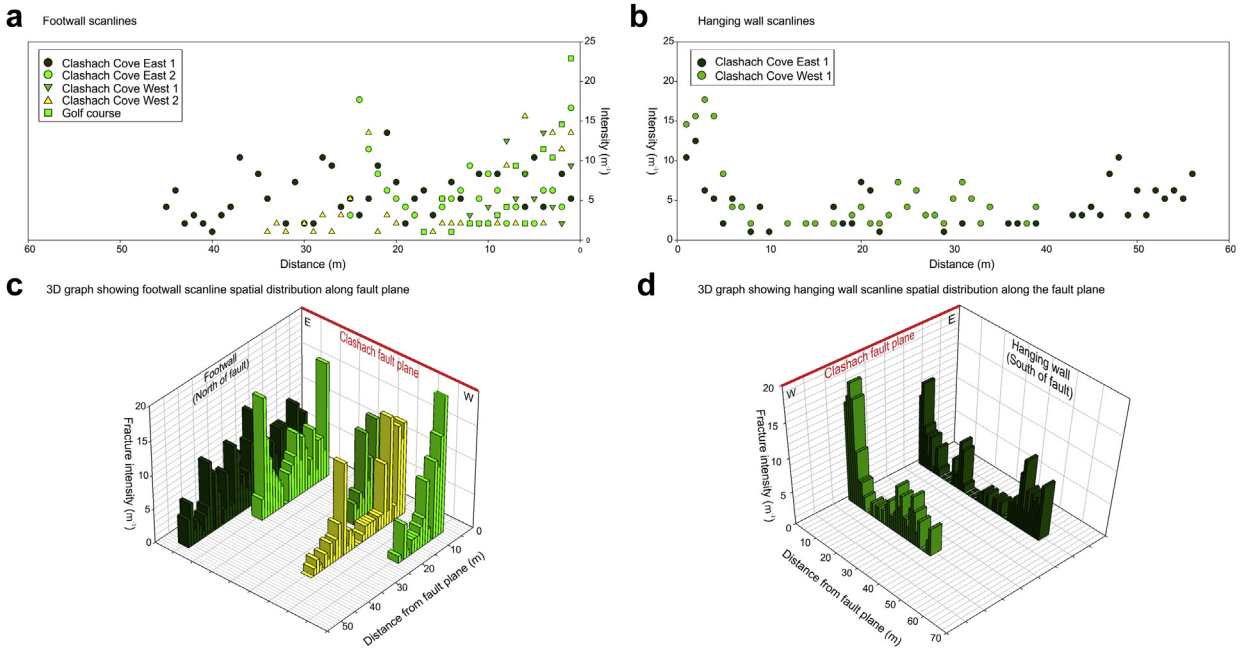

Fig. 3. a and b show 2D graphs showing intensities of cataclastic deformation bands measured along scan lines oriented perpendicular to the strike of the Clashach fault. Graph a) shows footwall deformation band intensities decreasing away from the fault plane. Graph b) shows hanging wall scan lines mostly decreasing away from the fault plane with some localised intensity peaks at ~50 m from the fault plane. Fig. 3c and d show 3D graphs of the same scanline data sets displayed spatially east to west along the fault strike.

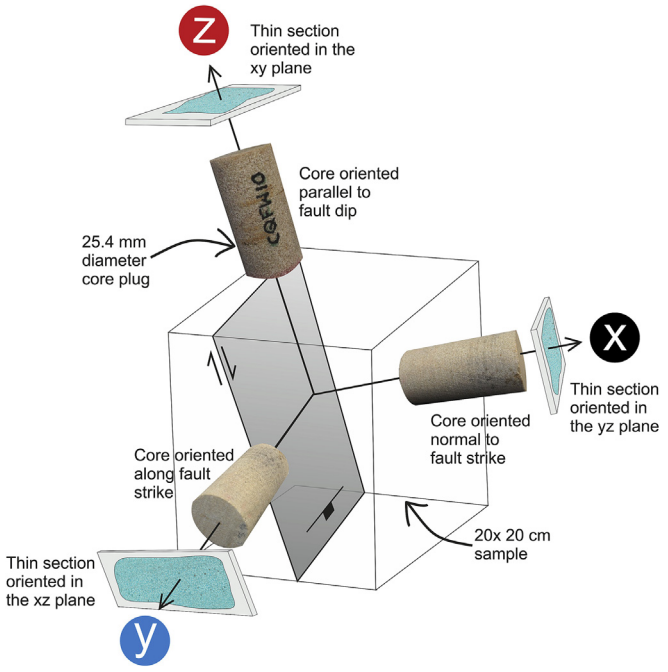

Fig. 4. Schematic diagram showing core plug and thin section orientations taken from each rock sample. The fault plane has been added to show the relative orientations of the cores and sections to the fault.

$$K = 2\mu Q(L/A)\left(P_2/(P_1 - P_2)^2\right)$$

An average gas pressure (P_{mean}) was calculated for each core plug from a range of input and output pressures. Measured permeability (mD) is then plotted against $1/P_{mean}$ (1/atm) with a line of best fit. The intersection of the plotted line with the y axis

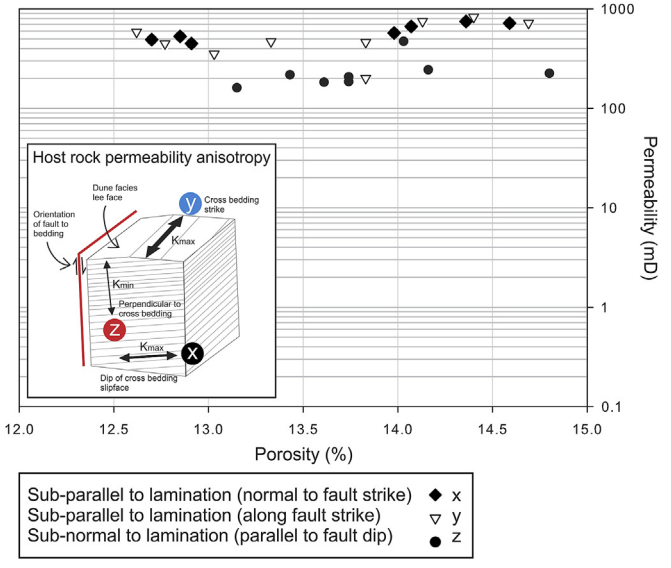

Fig. 5. Porosity–permeability cross plot showing permeability anisotropy in cores plugged from undeformed Hopeman Sandstone Formation host rock samples collected from the fault footwall. Cores have been sampled in three directions to the Clashach fault plane (x, y and z see Fig. 4). Maximum permeabilities are measured in x- and y-oriented core plugs which are parallel to sedimentary lamination. Minimum permeabilities are perpendicular to lamination in z-direction core plugs. Mean permeabilities are 570 mD and 515 mD in x and y oriented cores, over twice the mean permeability of 245 calculated from z-oriented cores.

(permeability) gives the permeability of the core plug with an applied Klinkenberg correction. The Klinkenberg correction allows gas permeability measurements to be correlated to the permeability of a core with a liquid flowing through it (Klinkenberg, 1941).

Permeabilities from 12 core plugs from four samples were measured at confining pressures between 10 and 100 MPa. In the confining pressure permeameter, core plugs are wrapped in heat shrink polyolefin tubing and confined in a pressure vessel by oil pressurised using a hand pump. A 5 min interval was allocated to allow core plugs to relax at each confining pressure before permeability was measured. Following precedent tests, three core plugs of variable orientations were left at high confining pressures (100 MPa) overnight to assess the influence of time dependent compaction on permeability (Faulkner and Rutter, 1998). Samples showed no change in measured permeabilities within 5 min of being confined and 24 h of confining pressure. Therefore any permeability decrease observed during increasing confining pressure may be attributed to the poroelastic response rather than grain crushing. Confining pressure permeability tests were also corrected for flow slippage of gas using a Klinkenberg correction (Tanikawa and Shimamoto, 2009).

Using these methods permeability is not measured directly but through the measurements of pressure, flow rate, viscosity and porosity, and therefore uncertainties about permeability results must be analysed considering variable uncertainties. Length and cross sectional area of each core plug is recorded from a mean of 10 caliper measurements accurate to 0.01 mm. Time (flow rate) is measured using a hand held stopwatch with human precision calculated as ±0.2 s. Pressure measurement uncertainty is ±0.1 psi, accuracy of viscosity ±0.2% (0.00034 cp calculated across a range of room temperatures), accuracy of gauges 0.1% of full scale accuracy 0–60 psig.

Core plug porosity was measured using a helium injection porosimeter. The core plug is put into a tight compartment and a known volume of He gas is injected from a different chamber at a defined pressure and the equilibrium pressure of the two chambers is recorded. This method uses the bulk volume of a core plug calculated from caliper dimensions to calculate grain volume and hence porosity.

Results

'Ambient' pressure permeability (low sleeve pressure < 2.8 MPa)

Steady state permeabilities of all 45 core plugs were measured in a low-pressure permeameter. Permeability results from core plugs in three orientations x, y and z are plotted on three corresponding graphs (Fig. 6a, b and c). In these graphs permeability is plotted on a log scale against sample location with respect to the fault plane in centimetres (0–50 cm). Results from samples collected from the footwall at all localities are plotted on the left on each graph, and hanging wall samples are plotted on the right following the orientation of fault architecture shown in Clashach fault cross sections (Fig. 2). Permeability data are plotted in SI units of metres squared (m^2) and also plotted in milliDarcies. Core plug permeabilities range between 0.02 mD and 300 mD.

All three graphs show that core plug permeabilities around the fault are considerably more heterogeneous than host rock permeabilities and range across five orders of magnitude (Fig. 6) compared to less than one order of magnitude (Fig. 5).

Permeability anisotropy in three orientations

Twelve cataclastic fault rock samples, each comprising of a set of three core plugs, show anisotropy of permeability in three orientations. The magnitude of anisotropy in each sample varies from less than 1 to more than 3 orders of magnitude (from 0.02 mD to

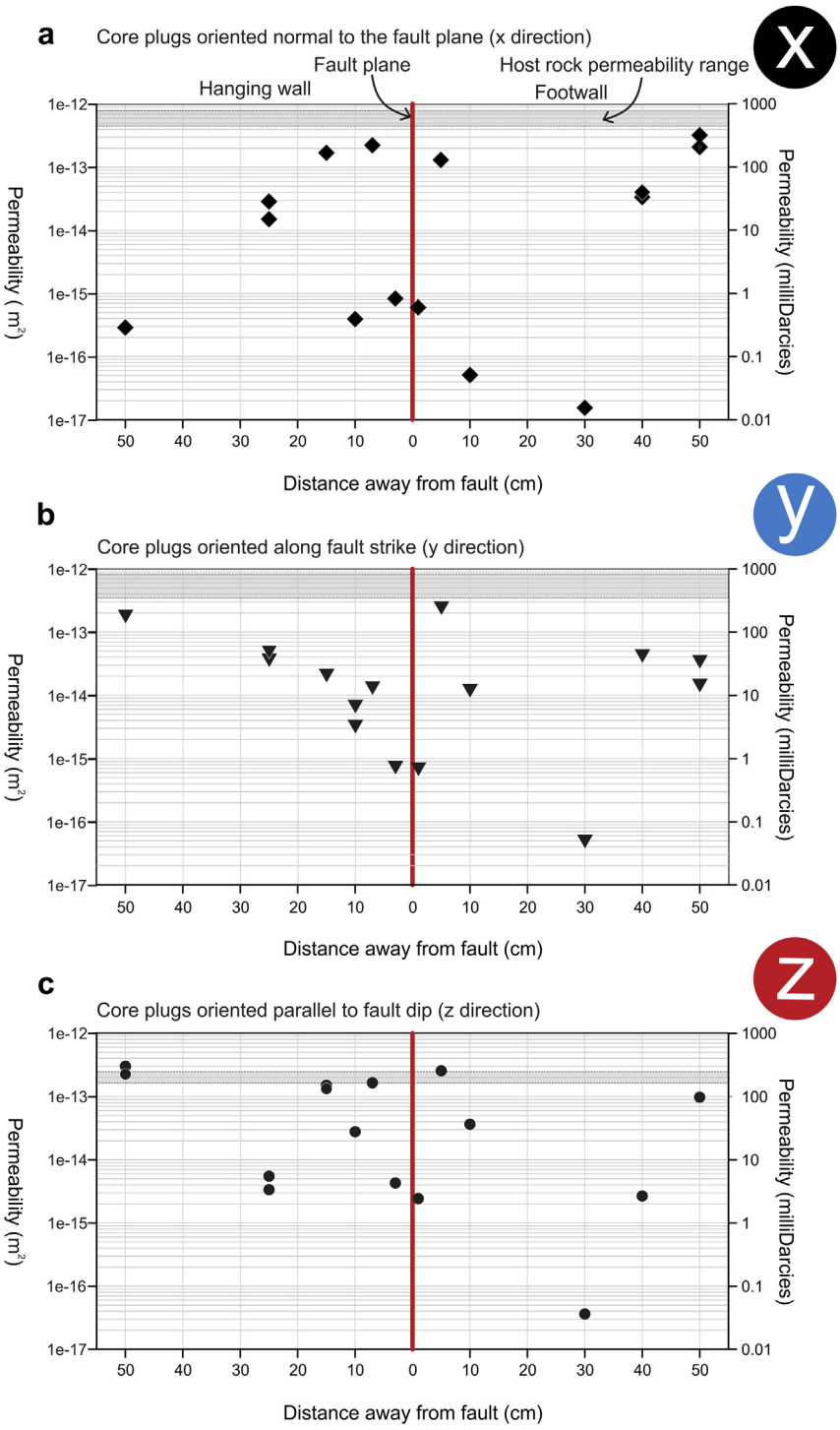

Fig. 6. Graphs display core plug permeabilities from 12 samples collected at a range of distances from the fault plane in the hanging wall and footwall. Samples were core plugged in three orientations to the fault plane and show anisotropy of permeability within single samples. Graph a) shows permeabilities of cores oriented normal to the fault plane (x) b) shows core oriented along fault strike (y) and c) shows core oriented parallel to fault dip (z). Permeability is measured using nitrogen as pore fluid at ambient pressures. Permeability heterogeneity is more pronounced between hanging wall samples than footwall and x-oriented cores are more heterogeneous than y- and z-oriented cores. Grey strips repeat the range of host rock permeabilities in each core plug orientation plotted in Fig. 5.

300 mD) with samples closer to the fault plane tending to show permeabilities ranging over 2 orders of magnitude. The orientation of the anisotropy is also variable, with 6 samples showing maximum permeability (K_{max}) down fault dip (z), 3 samples show K_{max} as along fault strike (y) and 3 samples with K_{max} normal to fault strike (x). To consider the *relative* permeability anisotropy between samples, the ratio of permeabilities is calculated between the three core plugs of each sample, and illustrated on a triangle plot (Fig. 7). On this plot the proportions of permeabilities from three perpendicular core plugs sum to 1. Anisotropic samples plot towards one of the triangle vertices depending on which orientation has the maximum permeability. Conversely if the permeabilities of three core plugs were about equal, i.e. isotropic permeability, they plot in the centre of the triangle. All 12 samples

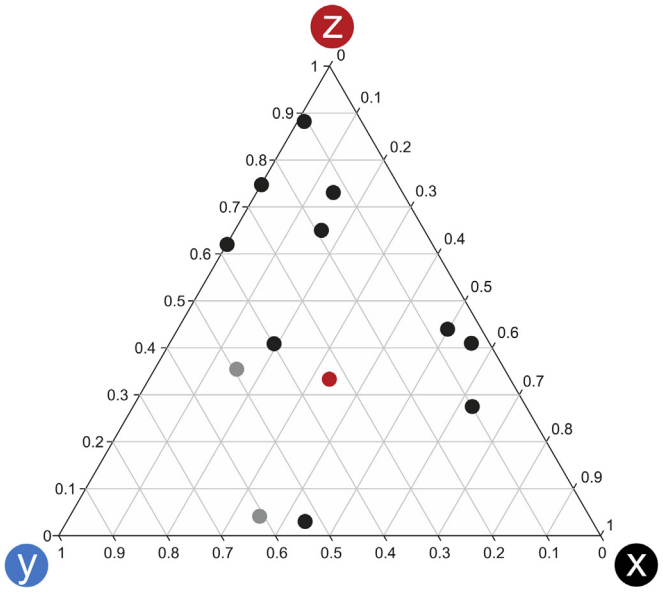

Fig. 7. Triangle plot showing the ratios of three core plug permeabilities. Cores are plugged from 12 samples in three orientations to the fault plane; x, y and z (see Fig. 4). All 12 samples show significant permeability anisotropy in three orientations with 5 samples showing maximum permeability in the down fault dip or z direction. Anomalous samples discussed in the results section are coloured grey. The triangle centroid is coloured red. (For interpretation of the references to colour in this figure legend, the reader is referred to the web version of this article.)

(36 core plugs) show anisotropic permeability and they plot towards the triangle sides and vertices (Fig. 7).

Permeability anisotropy in two orientations

Spatial patterns of preferential permeability orientations are highlighted by comparing core plug permeabilities in the two directions with respect to the fault kinematics: along fault strike (y) and parallel to the fault dip direction (z) (Fig. 8).

Seven samples located close to the fault plane (<20 cm) in both the hanging wall and footwall show maximum permeability (K_{max}) parallel to fault dip (z). In the footwall samples, these permeability values are 10 times greater than along fault strike (y). Five samples located further away from the fault plane (>20 cm) show variable magnitudes of anisotropy in differing directions of maximum permeability; two samples present z oriented K_{max} and three show y oriented K_{max}. Of the three samples which show maximum permeability along fault strike; one sample (25 cm into footwall) may be viewed as anomalous as there is a <2 mm thick cataclastic deformation band cutting obliquely across the core plug oriented parallel to fault dip (z). This localised low-permeability feature may have reduced parallel to fault dip core plug permeability as in previous studies (Shipton et al., 2002). Permeabilities from the sample collected 30 cm from the fault in the hanging wall could also be unreliable as the measurement precision of the ambient pressure permeameter is reduced at low permeabilities (<0.01 mD). Anomalous samples are coloured grey on the triangle plot (Fig. 7).

Reservoir pressure permeability (confining pressures 10–100 MPa)

Four cataclastic rock samples were selected for permeability measurement under reservoir pressures. Samples 1 and 2 were taken less than 10 cm into the footwall and hanging wall (measured from the fault plane), respectively and Samples 6 (footwall) and 11 (hanging wall) are from further away from the fault plane (Fig. 9a, b, c and d). Sample locations are marked on the geological map (Fig. 2). Over sixty permeability measurements were collected from each core plug. Permeabilities were measured at a range of confining pressures between 10 MPa and 100 MPa to reproduce the depth of faulting >1.5 km (~37 MPa) and simulate reservoir pressures up to 4 km of burial (100 MPa). After 100 MPa the confining pressure was decreased gradually and further permeability measurements taken on the down-pressure cycle, at the same confining pressures as those on the up–pressure cycle. Permeabilities were also taken at different pore fluid pressures between 0.1–0.6 MPa and 0.6–1 MPa. Each of the four graphs shows results from a single sample set of three cores (x, y and z plugs) at a fluid pressure of 0.6 MPa (Fig. 9a, b, c and d). Measured core plug permeabilities range between <0.0001 mD and >100 mD.

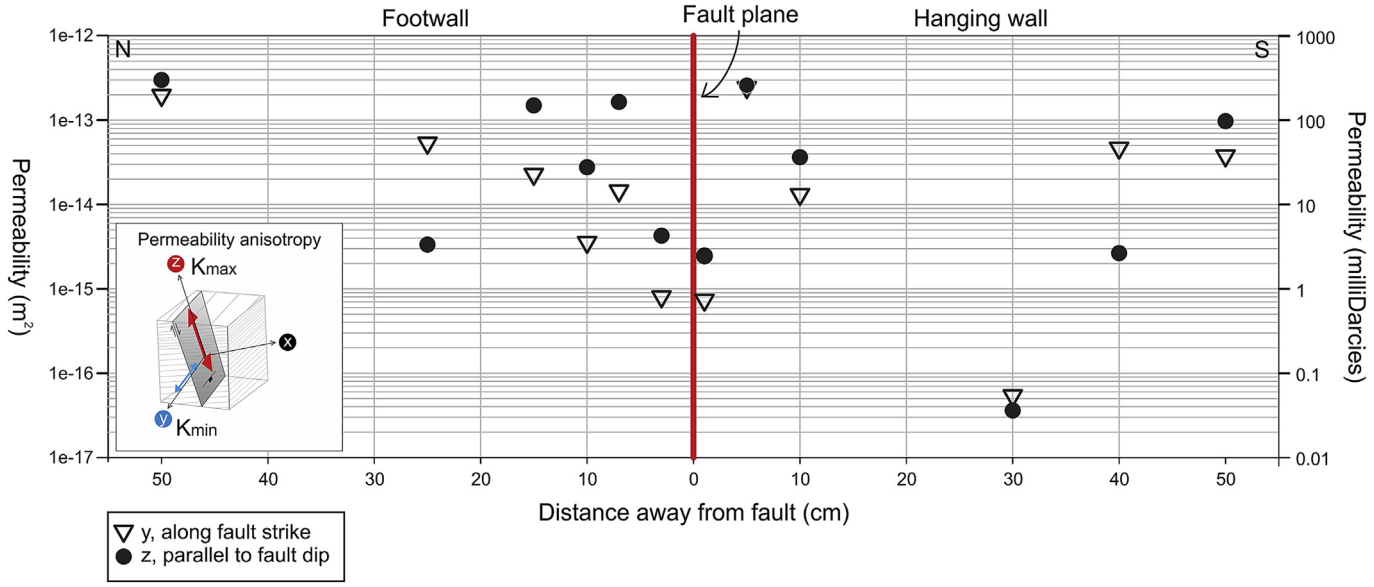

Fig. 8. Graph showing measured core plug permeability data in two orientations to the fault; down fault dip (z) and along fault strike (y). Maximum permeability is predominantly down fault dip in samples located close to the fault plane.

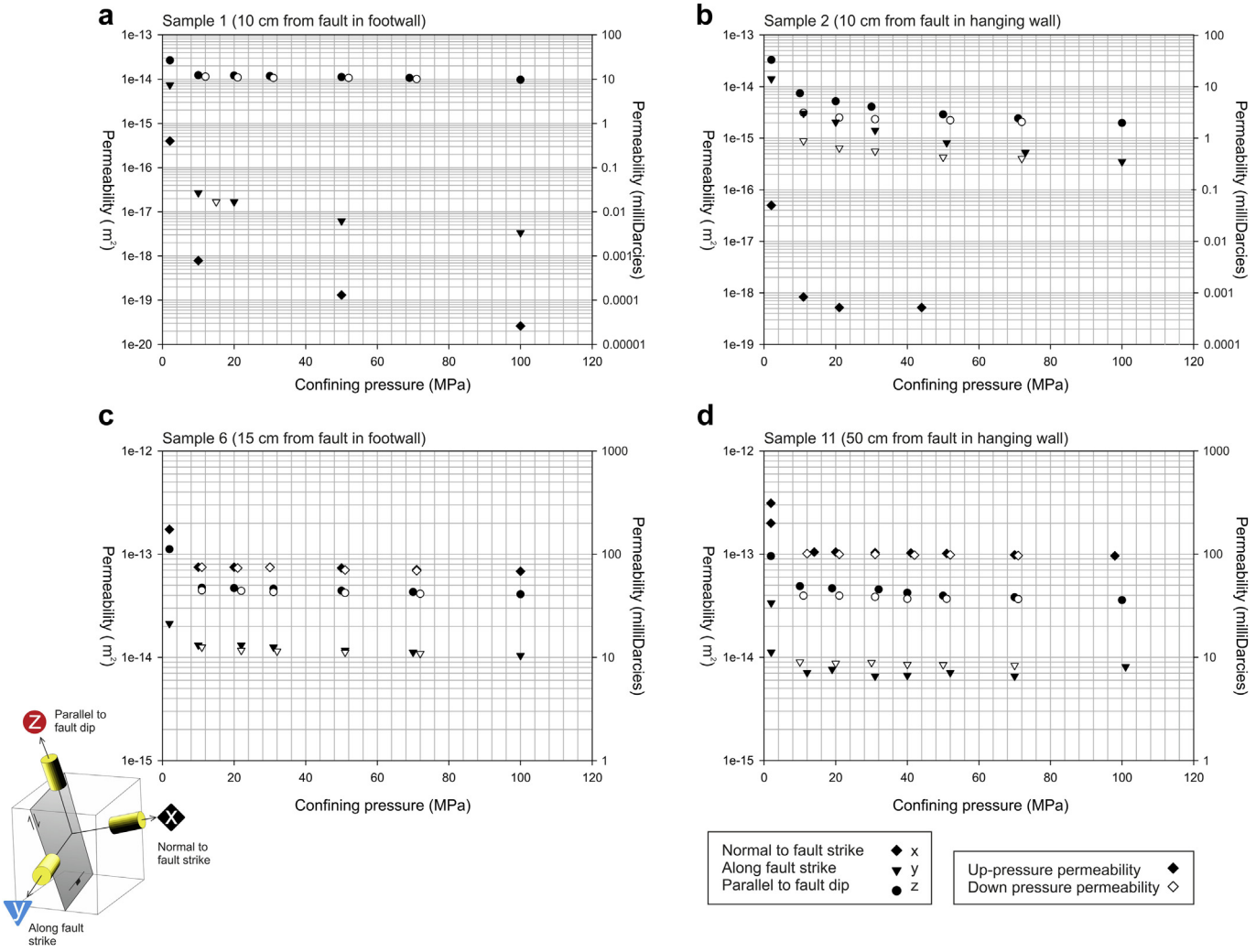

Fig. 9. Graphs showing permeability measurements of core plugs under reservoir confining pressures using N_2 gas as pore fluid. Each of the four graphs a – d display results from a single sample set of three cores; x, y and z at a fluid pressure of 0.6 MPa. Y-axis scales vary between graphs.

Correlation of permeabilities from ambient pressure (Fig. 6) and low confining pressure tests (10 MPa) show permeabilities in all cores decrease with confining pressure. The amount of reduction in permeability can depend on core plug orientation. Permeability reduction is largest (between 1 and 3 order of magnitude) in x- and y-oriented core plugs taken from samples close to the fault plane (Fig. 9 a and b). In contrast, permeabilities of z-oriented core plugs in these samples are less affected by confining pressure, decreasing by around half an order of magnitude compared to ambient pressure results. Variations in permeability reduction with increased confining pressure in core plugs of different orientations are less defined further from the fault plane (less than half an order of magnitude lower in permeabilities at ambient pressures and confining pressures of 10 MPa) (Fig. 9 c and d).

Trends of permeability across a range of confining pressures also vary depending on sample distance to the fault plane. As confining pressures are increased from 10 to 100 MPa permeabilities decrease by around half an order of magnitude in cores from samples taken less than 10 cm from the fault plane (Fig. 9 a and b). In comparison, the permeabilities of core plugs sampled further from the fault plane show small decreases with increased confining pressure (Fig. 9 c and d). Permeabilities measured at the same confining pressures both during pressurisation and depressurisation tend to show negligible permeability decrease in core plugs from footwall samples (Fig. 9 a and c). In contrast, some hanging wall core plugs show comparatively larger discrepancies between up- and down-pressure permeabilities of up to half an order of magnitude (Fig. 9b).

Permeability anisotropy in three orientations

Confining pressure permeability tests confirm permeability anisotropy in three orthogonal orientations in all four samples (Fig. 9). The magnitude of confining pressure permeability anisotropy is larger than the measured ambient pressure permeability anisotropy in the same sample. As with ambient pressure results, the degree of permeability anisotropy is highest close to the fault plane in both the footwall and hanging wall, over 5 and 4 orders of magnitude respectively (Fig. 9 a and b). In both these samples maximum permeability is parallel to fault dip (z), intermediate permeability is along fault strike (y) and minimum permeability is normal to the fault plane (x). In contrast footwall and hanging wall samples further from the fault plane show permeability anisotropy in three orientations just under and just over one order of magnitude respectively (Fig. 9 c and d). In these samples, maximum permeability is in the x-orientation, intermediate permeability is in

the z-orientation and minimum permeability is in the y-orientation.

Permeability anisotropy in two orientations

Permeability anisotropy in the two fault plane parallel orientations, show that z-oriented permeability is higher than y-oriented permeability in all four samples and at all confining pressures. The degree of anisotropy in two orientations is nearly 3 orders of magnitude close to the fault plane in the footwall (Fig. 9a) and just under one order of magnitude further from the fault plane in the footwall and in all hanging wall samples (Fig. 9 b, c and d). In comparison, ambient pressure permeability anisotropies in z and y-oriented fault parallel cores are under one order of magnitude in all four samples (Fig. 8).

Statistical variation of permeability in fault rocks

Repeat core plugs were taken from 25% of samples to investigate the heterogeneity of permeability in fault rocks (Fig. 6). The number of repeat cores was limited by the size of field samples and difficulties encountered in coring deformed rocks. However, the heterogeneity of permeability and porosity in a single core plug orientation was assessed in two large samples (50 × 50 cm) collected for statistical analysis more than 50 cm from the fault plane in the hanging wall and footwall at Clashach Cove west. Measured permeabilities and porosities from 7 z-oriented cores in a hanging wall damage sample show permeabilities ranging from 796 to 984 mD while z oriented permeabilities in 5 cores taken from a footwall damage sample shows permeabilities ranging from 430.7 to 557.1 mD (Fig. 10).

Porosity

Porosities of all 45 core plugs were measured using helium and are calculated as percentage porosity of the core plug volume. Porosities were also quantified from 36 corresponding thin sections using image analysis software.

Core plug porosity

Porosities from core plugs oriented in x, y and z directions are represented graphically with distance from the fault and also as *relative* proportions on a triangle plot (Fig. 11 a and b respectively). Porosities plot around the midpoint of the triangle and therefore porosities within three core plugs from each of the 12 samples are relatively homogeneous (isotropic). Although these data quantify the magnitude of bulk porosity in a core plug they provide no information regarding pore sizes, distributions, geometries or pore connectivity. These pore attributes can be investigated through image analysis on oriented thin sections.

Thin section porosity

Three polished thin sections were prepared orthogonal to the axis of each core plug (Fig. 4). In contrast to core plug measurements, porosity measured from 25 × 15 mm areas on these three thin sections show pronounced variations, ranging between 5 and 20% porosity within a single sample. Samples collected close to the fault plane (<10 cm) often show higher porosities in z corresponding thin sections. These relationships have been tested by sampling a range of areas to account for the heterogeneity of porosity on a thin section scale. The geometries of pores have been assessed using ImageJ software (Schneider et al., 2012) with preliminary results showing a preferential alignment of pore long axes in sections oriented orthogonal to x and y-oriented core plugs.

High resolution image analysis of microstructural features has been carried out on images derived from BSEM (Back-Scatter Electron Microscopy) and SEM-CL (Scanning Electron Microscope-Cathodoluminescence). Microstructural analysis has identified four main mechanisms which may alter porosity and in turn influence permeability. These microstructures include tectonic mechanisms of cataclasis (Fig. 12a), inter- and intra-granular microfracturing of grains (Fig. 12b), plus tectonically-related diagenetic mechanisms of pressure solution along grain boundaries (Fig. 12c) and associated quartz cementation (Fig. 12d). Contemporaneous formation of microfractures and cataclasis with extensional faulting is evidenced by cementation of open microfractures and cataclased grain clasts with the same luminescence quartz cement as is found in all thin sections made from samples taken close to the fault plane (Fig. 12d).

Interpretation

The porosities of 45 core plugs from 12 samples vary between 4% and 22% (Fig. 11a). Porosity variation between samples is affected by changes in microstructure and cementation depending on the sample proximity to the fault plane and location along fault strike. Within a single sample porosities are relatively homogeneous (Fig. 11b) with a maximum variation of less than 5% between

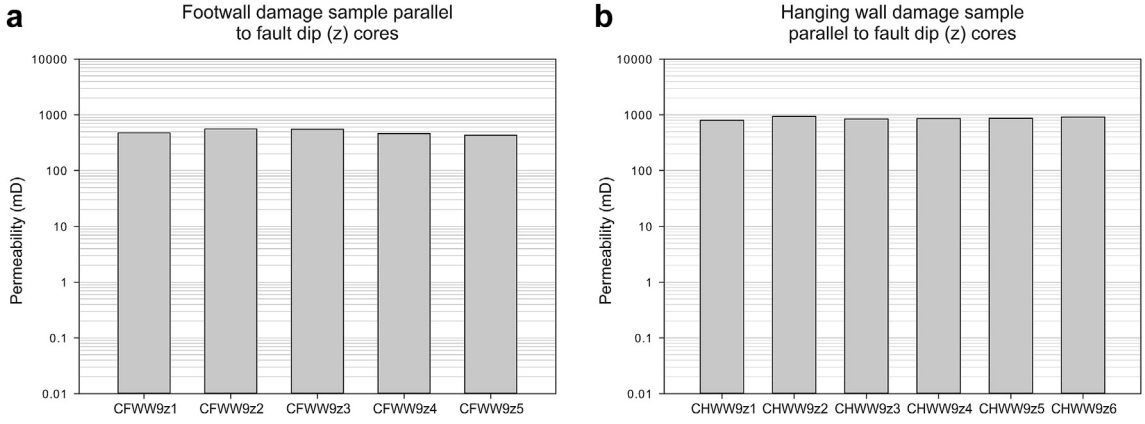

Fig. 10. Graphs showing the consistency of core plug permeability measurements taken in a single direction, down fault dip (z) from individual samples in both the hanging wall and footwall.

a set of three cores, therefore microstructures and cementation are considered to be consistent within a 20 × 20 cm sample scale. In contrast, 2D areal porosities derived from three orthogonal thin sections are seen to vary by up to 19% within a single sample. These findings strongly suggest that pores in faulted rocks have non-spherical (anisotropic) shapes and a degree of preferred orientation. We infer that the "cut effect" inherent in 2D thin sections is sampling more pore space in certain orientations (Fig. 13). Formation of these commonly oriented, and therefore anisotropic, intergranular pores through fault-related deformation mechanisms is interpreted as creating the fault rock permeability anisotropy measured around the Clashach Fault.

Anisotropic pores

The development of anisotropic pores and connected pore networks oriented at a low angle to the maximum principal stress (σ_1) can be visualised through 'the void cell model' (Li and Li, 2009). In this model, anisotropic pore structures with long axes oriented perpendicular (or at a high angle) to the maximum principal stress are weak and will collapse under increasing differential stress, leaving the more stable elongate pores (oriented at lower angles to σ_1) open, and thereby available to dominate the bulk porosity (Fig. 14a and b). This scheme for porosity evolution has been shown in DEM modelling for unconsolidated materials (Kang et al., 2012),

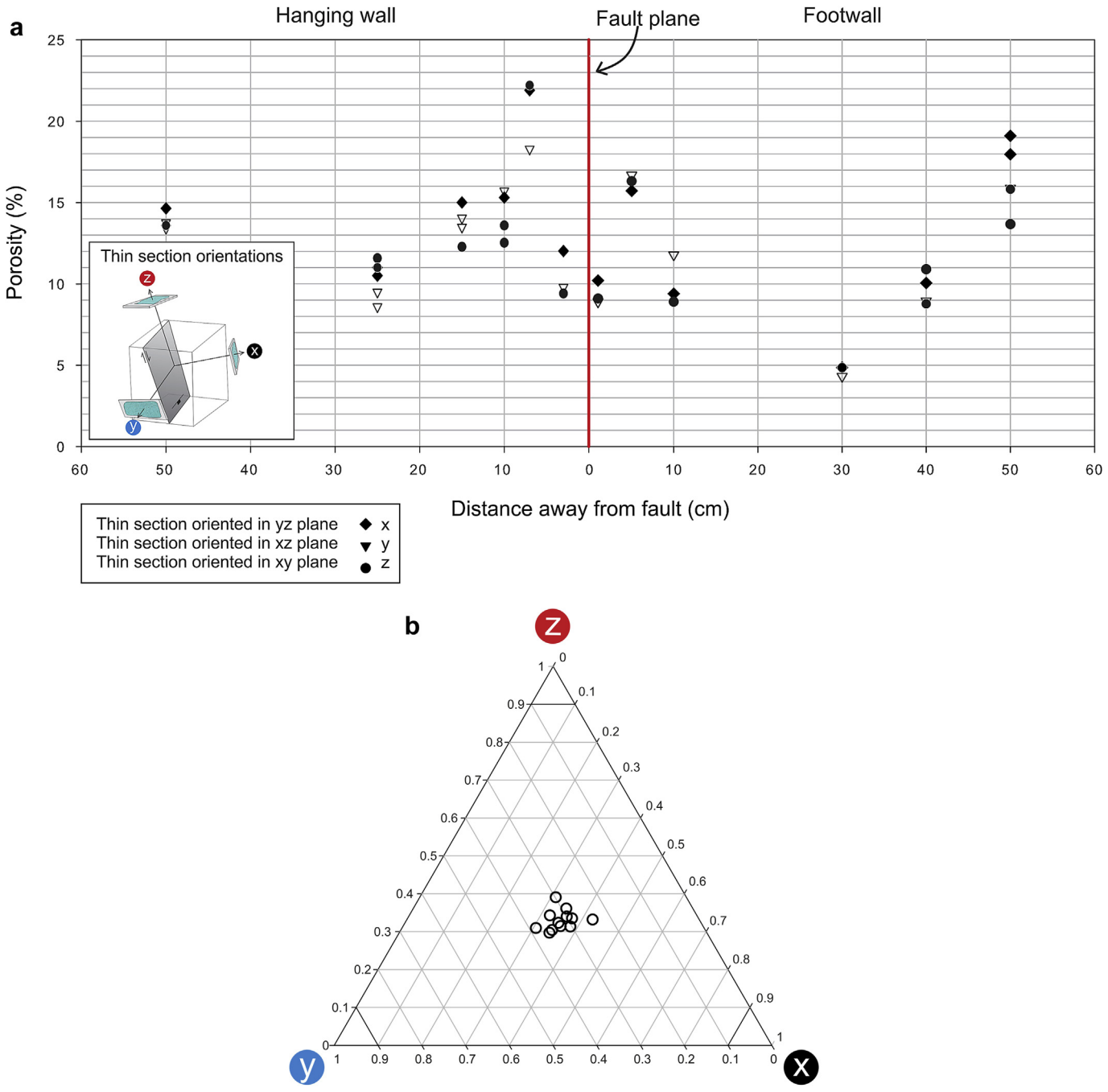

Fig. 11. a. Graph showing core plug porosities measured from thin sections. Results show variations in area porosity of up to 15% within fault rock sample. b. Triangle plot showing ratios of core plug porosities from single samples oriented in x, y and z orientations are relatively homogeneous and plot near the triangle midpoint.

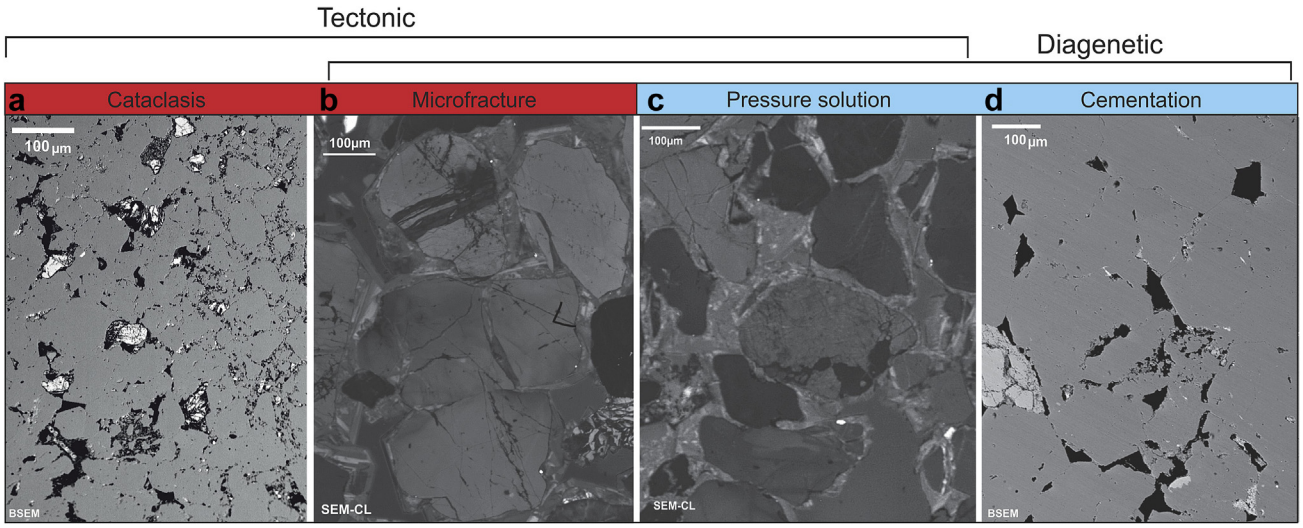

Fig. 12. Micrographs showing four main porosity altering, microstructural features derived from high resolution Back-Scatter Electron Microscope images (BSEM) (Fig. 12a and d) and Scanning Electron Microscope-Cathodoluminescence images (SEM-CL) (Fig. 12b and c).

but could also apply in consolidated granular rocks as cemented grains are quasi-continually broken apart by cataclasis, the dominant deformation mechanism identified in most studies of deformed porous sandstones (e.g. Saillet and Wibberley, 2010; Fossen et al., 2007; Aydin, 1978). The mechanics and kinematics of grain-scale cataclasis involve an initial dilatancy to allow for grain breaking, including some shearing, followed by reorganisation of grains and subsequent compaction (Antonellini and Aydin, 1994). Episodes of dilatancy in developing fault rocks could allow for the development of new pore space, which is then only preserved if oriented sub-vertically so that it is stable against the maximum principal stress (30° from the down fault dip direction in a normal fault), while compaction and destruction of unfavourably oriented pores would occur perpendicular to the maximum principal stress. This process would form well connected permeability pathways sub-parallel to σ_1 (z-orientation) and reduce permeability parallel to σ_2 and σ_3 as observed in permeability results from this study. Minimum permeability is often identified in y-oriented core plugs. Faulted sandstone may also behave anisotropically in the x and y directions due to differences in the lateral packing of grains. During normal faulting the stress ratios between vertical and the two horizontal stresses are variable; $\sigma_1-\sigma_2$ is smaller than $\sigma_1-\sigma_3$, therefore grain scale deformation along fault strike (y-direction) may be more compressive, while grain scale deformation response normal to the fault (x-direction) is more dilative.

Pervasive, distributed cataclasis identified in the samples used in this study is evidenced by grain comminution in thin sections. These cataclasites are visibly homogeneous in hand sample and have no sedimentary lamination as it has been destroyed by cataclasis. Distribution of localised cataclasis can also be observed around the Clashach fault on a meso scale as cemented cataclastic deformation bands. As the spatial intensity of localised cataclastic deformation bands increases towards the fault plane (Fig. 3), we infer that the quantity of preferentially-oriented and connected pores – and therefore permeability anisotropy – observed in samples of homogenous cataclasis also increases towards the fault plane (Fig. 14c and d). The distribution of deformation bands along strike of the Clashach Fault is also variable, probably due to its segmented geometry at a larger scale, with short lengths (<5 m) of anastamosing deformation bands overlapping and intersecting to form discontinuous units of cataclasite along fault strike (Torabi and Fossen, 2009). In contrast, when viewed in cross section, deformation bands are very straight and continuous (>20 m) with variations in orientation only when they are apparently refracted between dune sets (Fig. 14d). It is inferred that this continuity of deformation bands in the down fault dip direction may also form quasi-continuous, highly-connected pore networks from elongate oriented pores produced during cataclasis.

Microfractures

Previous studies have shown that fault-related microfractures form with their long axes parallel to the principal maximum stress (Anders and Wiltschko, 1994; Vermilye and Scholz, 1998). Although the percentage porosity of microfractures is negligible on a thin section scale in Clashach Fault samples, the *connectivity* of preferentially oriented elongate pores may be enhanced by the preferential orientation of microfractures aligned parallel to the maximum principal stress at the time of faulting. Previous studies show that increasing confining pressure during permeability tests tends to close any open microfractures, including both tectonic uplift related fractures and fault related microfractures (Armitage et al., 2011), thereby reducing core plug permeability. Our results show that all core plug permeabilities decrease with increasing

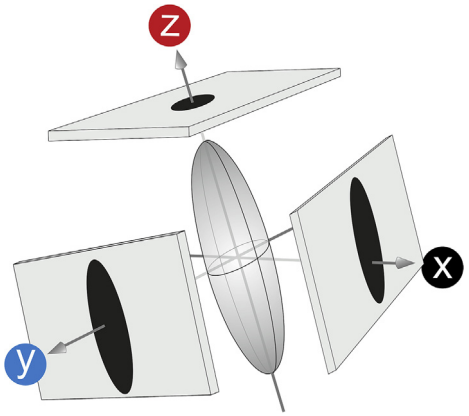

Fig. 13. Schematic diagram showing area porosity sampling bias inherent in 2D thin sections through non-spherical features such as elongate, oriented pores.

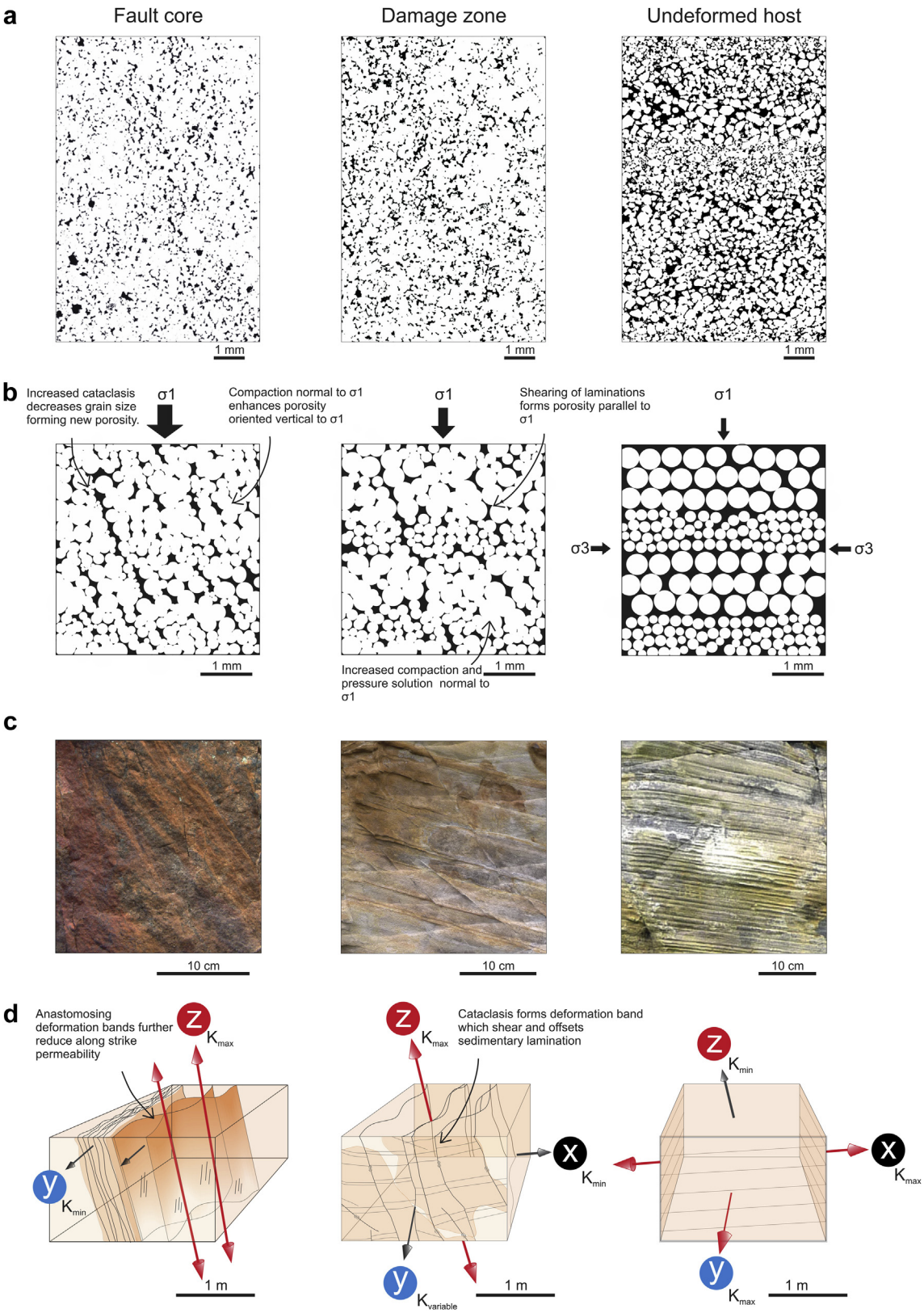

Fig. 14. Shows evolution of the internal structure of porous sandstone with increasing fault deformation (from undeformed host rock to fault core) and the relationship to permeability anisotropy. Vertically, Fig. 14a–d show corresponding images and models from grain scale to macro field scale. a) shows thin sections images showing grain-scale change in porosity and pore shapes with increasing deformation (from right to left). Images are thresholded with black areas showing porosity and white areas showing grains and quartz cement. b) presents models for the development of anisotropic pores and connected pore networks oriented at a low angle to the maximum principal stress (sigma1). c) comprises photographs showing increasing spatial intensity of cataclastic deformation bands and destruction of sedimentary lamination towards the fault plane (right to left). d) presents models of increasing cataclasis towards the fault plane marked by increased intensity of deformation bands and development of anisotropic permeability with maximum permeability oriented down fault dip.

confining pressure, but the permeability of core plugs from samples taken near to (<10 cm) from the fault plane (Fig. 9a and b) decrease more in comparison to samples taken further away (Fig. 9c and d). This finding is consistent with there being more microfractures to close in the samples near to the fault plane (Fig. 9). The permeability anisotropy observed in confining pressure tests is consistent with the ambient pressure results indicating that structures contributing to fluid flow pathways are being closed in all three core plug orientations i.e. their response to pressure is isotropic. However, in both samples located near to the fault plane (Fig. 9 a and b) permeability anisotropy becomes more pronounced, increasing 100 times to between 4 and 5 orders of magnitude. This is due to variable permeability decrease in cores of different orientations. In these samples, the permeabilities of core plugs oriented normal to fault strike (x) and along fault strike (y) are between 10 and > 100 times lower than at ambient pressures, while permeabilities of cores oriented down fault dip (z) are only 5 times lower. Variations in pressure sensitivity in cores of foliated gouge oriented parallel and perpendicular to a slip zone are have also been discussed in previous studies (Wibberley and Shimamoto, 2003). Differences in the effects of confining pressure depending on core orientation may be due to variations in the number of open microfractures in each core or variations in the contribution of open microfractures to core plug permeability. If microfractures dominate permeability in x- and y-oriented core plugs, closure of these elastically compliant flow pathways with confining pressure leaves only incompressible oriented pore pathways to conduct flow therefore enhancing the z-direction permeability (Fig. 15).

Discussion

In this study laboratory based measurements of permeability in samples of cataclasite from around a normal fault have provided an improved understanding of permeability anisotropy (magnitude and orientation) and permeability heterogeneity within the framework of the fault zone. In comparison with previous studies of fault rock permeability anisotropy in sandstones (Shipton et al., 2002; Saillet and Wibberley, 2013; Cavailhes et al., 2013), results from our study are unique in showing anisotropy of permeability in three orientations to the fault plane. Permeability anisotropy in three orientations has previously been measured in granite-hosted thrust faults (Evans et al., 1997) and phyllosilicate rich fault gouge from a strike-slip fault (Faulkner and Rutter, 1998; Wibberley and Shimamoto, 2005).

Direction of maximum permeability

An objective of this study was to investigate permeability anisotropy of porous fault rocks in the context of the fault kinematics and to consider whether structures controlling the properties of permeability are repeatable in other porous sandstone hosted faults in extensional or other structural settings. It should be noted, in this study only three core orientations have been cored – within a reference frame of the fault – therefore permeabilities outside this reference frame may vary. Previous theoretical work has suggested that the direction of maximum permeability (K_{max}) around normal faults should be sub-horizontal and parallel to the σ_2 direction, i.e. along fault strike (y), and parallel to the intersections between faults and microstructures such as microcracks (Sibson, 2000). However, permeabilities from samples collected near the fault plane in this study show the orientation of maximum permeability lies parallel to the fault plane and is predominantly parallel to fault dip (z). Assuming Andersonian stress conditions during normal faulting, this would mean K_{max} is oriented at about 30° to the sub-vertical maximum principal stress (σ_1) during faulting. Experimental tests measuring permeability on similar consolidated sandstone core plugs during deformation have shown maximum permeability occurs in the direction of maximum principal stress (Zhu et al., 2002). An example of inherent maximum permeability parallel to the slip direction measured on naturally deformed rocks confined at high pressures under static conditions in an isotropic stress field is shown in a study on cores sampled around a thrust fault in crystalline host rocks (Evans et al., 1997). The microstructures controlling the direction of maximum permeability in these studies are interpreted as preferentially aligned microcracks and porosity enhanced by fracturing and cataclasis formed during faulting (Evans et al., 1997) and during deformation in laboratory experiments where fractures are opening parallel to σ_1 (Zhu et al., 2002). These deformation mechanisms are believed to be responsible for altering porosity and pore

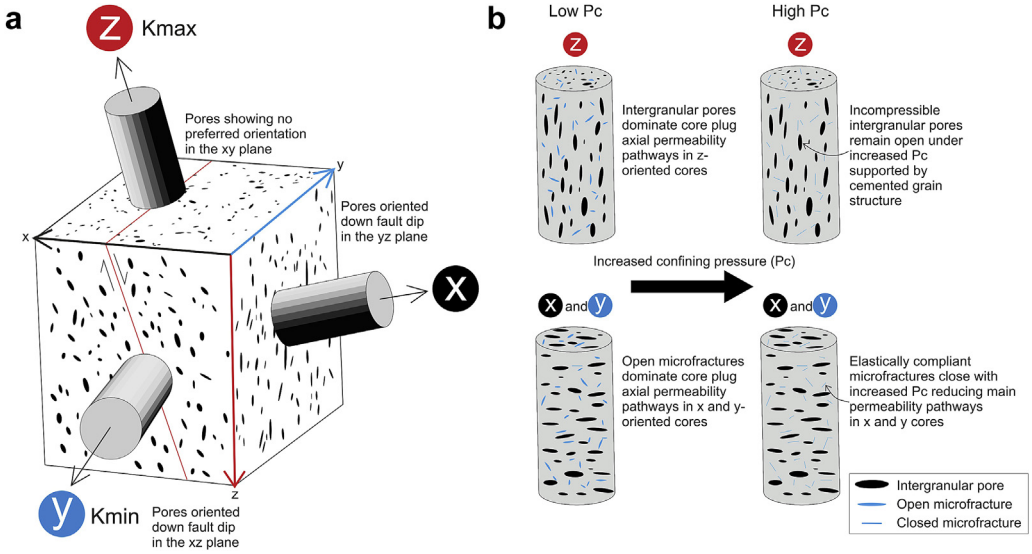

Fig. 15. a Shows a schematic diagram of maximum and minimum permeability pathways in faulted cataclastic sandstone, controlled by the formation of anisotropic pores. b. Explains the possible role of core plug orientation relative to anisotropic pore orientations in variable permeability sensitivity observed in at high confining pressures in Fig. 9.

connectivity. In a similar way, we propose a process by which fault-related pores and cracks oriented quasi-parallel to the maximum principal stress become the dominant porosity after 'the void cell model' (Li and Li, 2009). Other field-based studies of permeability anisotropy in foliated fault rocks show maximum permeability oriented perpendicular to the inferred direction of maximum principal stress during strike-slip faulting (Faulkner and Rutter, 1998; Wibberley and Shimamoto, 2005) and normal faulting (Cavailhes et al., 2013). These authors suggest that permeability anisotropy is controlled by preferential flow between phyllosilicate foliations intersecting with veins or Reidel fractures. Undeformed protoliths for the fault rocks in both of these studies included some phyllosilicate minerals, with more formed during faulting and the formation of fault gouge. Important differences between the orientations of the maximum permeability relative to the maximum principal stresses active during faulting in different studies may be due to variations in the dominant deformation mechanisms active in different host rock lithologies. The control of protolith lithology and fault rock type is illustrated in a new model contrasting the development of anisotropy in fault gouges formed in argillaceous rocks and cataclasites formed in sandstones (Fig. 16). Fault gouges formed in argillaceous rocks produce maximum permeability parallel to phyllosilicate foliation and fault fracture intersections and generally parallel to σ_2 (Fig. 16a). On the other hand anisotropy in sandstone cataclasites is developed by grain breakage and reorganisation creating anisotropic pore structures and dilatant microfractures, producing maximum permeability sub-parallel to σ_1 (Fig. 16b).

Variations in the direction of maximum permeability in the context of fault kinematics may also be influenced by the age of the fault and development of structures throughout the duration of active faulting. Older and/or more active faults will likely have a complex history of healing stages that could transform preferential permeability pathways operating during and after faulting. Previous work has suggested that this complexity of healing could account for variable fluid flow patterns observed around faults with different displacements (Fisher, 2001). Changes in permeability anisotropy during the early stages of fault evolution could be tested on large samples faulted in the laboratory, and then cored to test permeability in three orientations. Permeability anisotropy of faults in various stages of evolution is relevant to faults in reservoirs as the initial permeability structure post-faulting will have influenced the current in situ permeability patterns.

Degree of anisotropy

Results from this study show the degree of permeability anisotropy at ambient pressures is between 1 and 3 orders of magnitude from all samples, with anisotropies of 2 orders of magnitude in the majority of samples taken within 10 cm of the fault plane. The application of confining pressure to close microfractures reduces the overall magnitude of permeability, but it also enhances the magnitude of permeability anisotropy by 100–1000 times (4 and 5 orders of magnitude in samples collected $<$ 10 cm from the fault plane). These findings support the interpretation that permeability pathways in down fault dip (z) oriented cores are dominantly controlled by a less compressible network of pores oriented along the core plug axis (z) while much of the permeability in normal to fault plane (x) and along fault strike (y) oriented cores is dominantly controlled by elastically compliant microfractures. The increase in permeability anisotropy with confining pressure cannot be compared with previous studies due to the incompleteness of the various data sets, however it is noted that there is bigger decrease in permeability of low permeability protolith samples compared to high permeability faulted samples in crystalline granite (Evans et al., 1997) which also suggests the formation of a less compressible pore network through cataclasis. In their thrust fault study, Evans et al. (1997) found that permeability anisotropy in three orientations at ambient pressure is $>$ 4 orders of magnitude in cataclased fault core rocks and $<$2 orders of magnitude in fault damage rocks.

Heterogeneity of anisotropy

In this study core plugs oriented normal to the fault plane display the maximum permeability orientation in three samples (two $<$ 20 cm from the fault plane). These results are in contrast to the findings of previous studies around thrusts, strike-slip and normal faults that identify minimum permeabilities from cores oriented normal to the fault plane (x) (Evans et al., 1997; Faulkner and Rutter, 1998; Cavailhes et al., 2013). Overall the range of sample permeabilities from x, y and z oriented core plugs are variable within this study, however the range of permeabilities of normal-to-fault plane (x) core plugs is considerably more variable than that of cores oriented parallel to the fault plane (y and z). The heterogeneity of normal-to-fault permeabilities from previous studies is within the overall core plug variation (within one order of magnitude same as other core plug directions) (Cavailhes et al., 2013), or is unquantifiable due to low sample numbers in this orientation (Evans et al., 1997; Faulkner and Rutter, 1998). The normal-to-fault plane heterogeneity around Clashach Fault might be due to high permeability normal to fault pathways such as strike-normal joints observed in the field. Alternatively, it could be due to remnants of sedimentary laminations as the deformation mechanisms creating high permeability pathways are not evenly distributed and have been shown to localise in other studies (Fossen et al., 2007). This heterogeneity is unlikely to be replicable in an experimental setting as the samples used in this study are collected from four localities along fault strike, each showing different deformation intensities. However it is important to describe these heterogeneities from field samples, as faults encountered in reservoirs may also show deformation variation along a single fault.

Relevance of results, accuracy, and scaling issues

The use of 25.7 cm^3 core plugs is considered a valid sample size to measure permeability controlled by features of the order of 300 μm in length. However small core plugs can exclude the effects of large fractures and deformation bands on permeability data, therefore data from this study probably underestimates the bulk permeability around Clashach Fault. Fracture intensity scanlines could be put into a numerical reservoir model to account for this permeability. Further investigation of the extent and continuity of pore-scale, high-permeability pathways could be addressed through increasing the sample scale and measuring permeability anisotropy on larger core plugs. Previous studies of permeability in cataclased porous sandstones have suggested that at an increased scale fluid can just flow around permeability barriers like deformation bands and therefore have limited impact on reservoir scale permeabilities (Fossen et al., 2007). However in this study the main control on permeability is considered to be permeability conduits formed by oriented pores rather than permeability barriers. Assuming the formation of deformation-produced porosity is only dependant on the amount of deformation acting on a rock and that subsequent pore networks formed are relatively homogeneous, these pore scale features should

replicate the same permeability anisotropy results regardless of sample size.

The results of this study show that permeability anisotropy persists at high confining pressures representative of reservoir conditions, therefore these results are considered relevant to analogous faults in reservoir settings. Permeabilities measured from a 25.7 cm^3 core plug cannot be directly compared with borehole logging measurements of permeability or reservoir model scale permeabilities, as the measurement sensitivity varies with volume. Therefore we see scope to include these pore geometries and transport properties into upscaled reservoir models. To compare with active basins it would also be good to test the permeability patterns of core plugs within a normal fault stress field to see whether this would enhance or limit permeability anisotropy in Clashach Fault rocks.

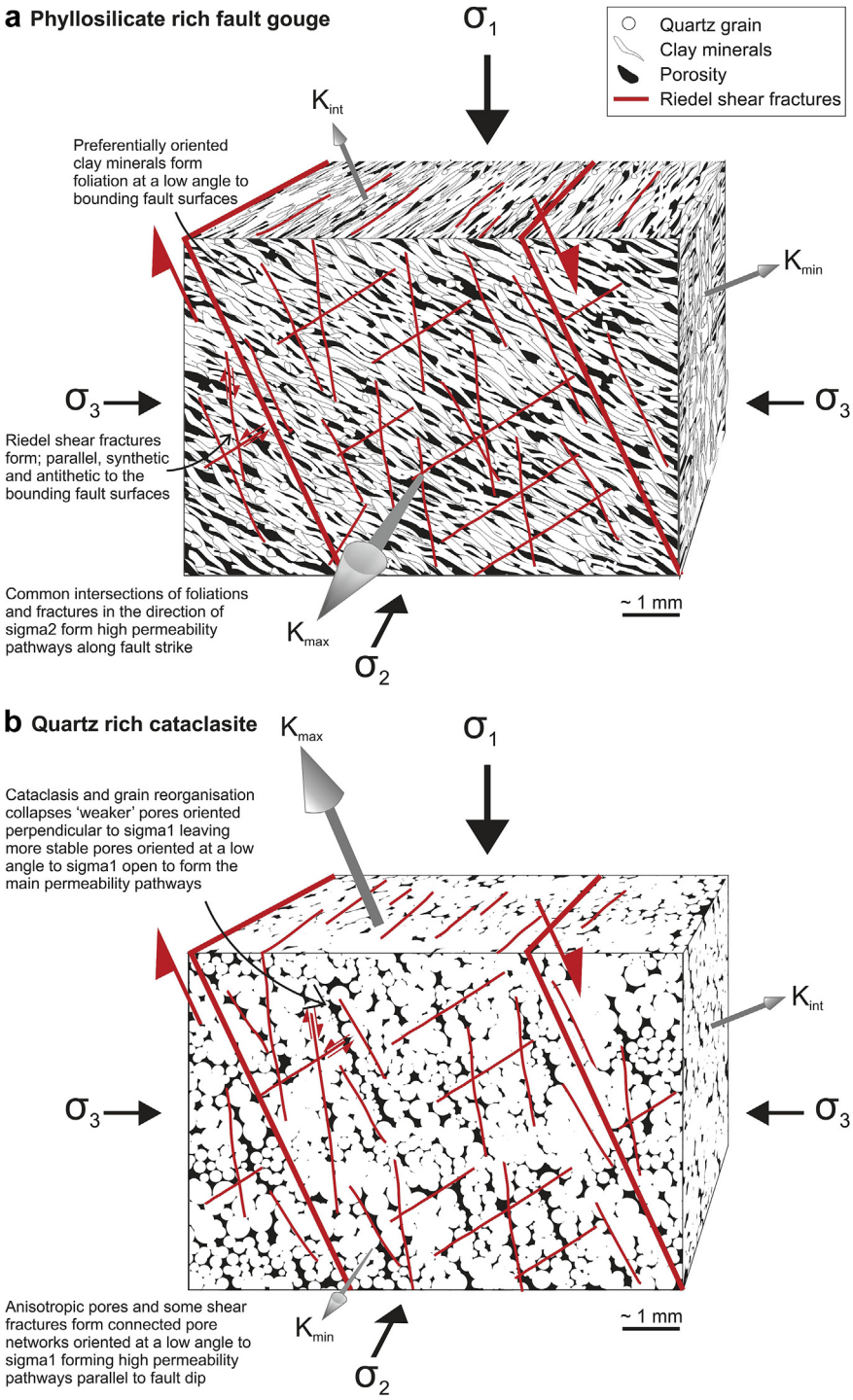

Fig. 16. Models showing stress induced microstructures which form permeability anisotropy around faults in two differing protolith lithologies. Fig. 16a illustrates the development of anisotropic permeability in faulted host rocks containing argillaceous components. Maximum permeability in the fault gouge is oriented parallel to $\sigma 2$, along common intersections of phyllosilicate foliation and shear fractures (after Faulkner and Rutter, 1998; Wibberley and Shimamoto, 2005; Cavailhes et al., 2013). Fig. 16b shows the development of anisotropic permeability in faulted quartz rich, porous sandstone protolith. Maximum permeability in the cataclastic fault rocks is oriented at a low angle to $\sigma 1$, along anisotropic pores structures and dilatant microfractures.

Summary and conclusions

It is commonly assumed that porosity and permeability will decrease with increased deformation in porous sandstone. However, deformation can have a permeability enhancing effect on fault rocks as the creation of permeability anisotropy can form permeability contrasts which – although bulk permeability is reduced – will enhance flow (Fossen et al., 2007). Core plug permeability tests carried out at ambient and confining pressures (up to 100 MPa, > 3 km burial depth) show that permeability is anisotropic in three orientations in 12 samples collected around a normal fault in porous sandstone. Maximum permeability is often parallel to fault dip (z), particularly in samples located close to the fault plane (<10 cm). In a normal fault this means that maximum permeability is at a low angle to the orientation of maximum principal stress. Permeability anisotropies within a single sample range up to 5 orders of magnitude, however the porosities of three core plugs from a single sample are relatively homogeneous. In contrast, area porosities calculated from core plug corresponding thin sections are very variable within a single sample implying that fault rock pores are shaped and oriented and variation in area porosity within three thin sections is due to a sampling bias or cut effect. The full results of fault rock porosity quantification will be published in future work, but this study provisionally concludes that a network of elongate pores oriented at a low angle to the maximum principal stress (down fault dip, z) is formed through deformation mechanisms of cataclasis and shearing. Combined with increased deformation, compaction and pressure solution of pores and grains oriented normal to the maximum principal stress, these elongate pores become the dominant pore network making preferential permeability pathways parallel to fault dip. The results from this study indicate that patterns of permeability around faults in porous rocks can be quantified at high resolution (centimetre scale core plugs) and that incorporating these results into reservoirs models will improve our understanding of fluid flow and pore pressure changes around faults in the subsurface.

In summary, we show that the formation of fault related micro-scale deformation structures can alter the host rock depositional porosity organisation supporting our hypothesis that this will create new permeability pathways measurable on core scale samples.

Acknowledgements

Thank you to Total E & P UK for funding the project, and especially Chris Wibberley, Claude Gout and Stephane Vignau for input. The author would also like to thank Zoe Shipton and Graham Yielding for their constructive reviews of the manuscript. Thanks also to Manuel Prieto for sharing his MSc pilot study written at the University of Aberdeen, Professor Martin Lee and Peter Chung at the University of Glasgow for SEM use and lastly thank you to Gavin Tennent for access to the Clashach Quarry and for samples.

References

Al-Hinai, S., Fisher, Q.J., Al-Busafi, B., Guise, P., Grattoni, C.A., 2008. Laboratory measurements of the relative permeability of cataclastic fault rocks: an important consideration for production simulation modelling. Mar. Petrol. Geol. 25, 473–485.
Anders, M.H., Wiltschko, D.V., 1994. Microfracturing, palaeostress and the growth of faults. J. Struct. Geol. 16, 795–815.
Antonellini, M., Aydin, A., 1994. Effects of faulting on fluid flow in porous sandstone: petrophysical properties. AAPG Bull. 78, 355–377.
Armitage, P.J., Faulkner, D.R., Worden, R.H., Aplin, A.C., Butcher, A.R., Iliffe, J., 2011. Experimental measurement of, and controls on, permeability and permeability anisotropy of caprocks from the CO_2 storage project at the Krechba Field, Algeria. J. Geophys. Res. 116, B12208.
Aydin, 1978. Small faults formed as deformation bands in sandstone. Pageoph 116.
Benton, M.J., Walker, A.D., 1985. Palaeontology, taphonomy and dating of Permo-Triassic reptiles from Elgin, North-east Scotland. Palaeontology 28, 207–234.
Berridge, N.G., Ivimey-Cook, H.C., 1967. The geology of the geological survey borehole at Lossiemouth, Morayshire. Bull. Geol. Surv. Gt. Br. 27, 155–169.
Caine, J.S., Evans, J.P., Forster, C.B., 1996. Fault zone architecture and permeability structure. Geology 24, 1025–1028.
Cavailhes, T., Sizun, J.P., Labaume, P., Chauvet, A., Buatier, M., Soliva, R., Mezri, L., Charpentier, D., Leclere, H., Trave, A., Gout, C., 2013. Influence of fault rock foliation on fault zone permeability: the case of deeply buried arkosic sandstones (Grés d'Annot, SE France). AAPG Bull. 97 (7), 1521–1543.
Chester, F.M., Logan, J.M., 1986. Implications for mechanical properties of brittle faults from observations of the Punchbowl fault zone, California. Pure Appl. Geophys. 124 (1–2), 79–106.
Edwards, H.E., Becker, A.D., Howell, J.A., 1993. Compartmentalisation of an aeolian sandstone by structural heterogeneities: Permo-Triassic Hopeman Sandstone, Moray Firth, Scotland. In: North, C.P., Prosser, D.J. (Eds.), Characterisation of Fluvial and Aeolian Reservoirs, pp. 339–365. Geological Society Special Publication 73.
Evans, J.P., Forster, C.B., Goddard, J.V., 1997. Permeabilities of fault-related rocks and implications for fault-zone hydraulic structure. J. Struct. Geol. 19, 1393–1404.
Faulkner, D.R., Rutter, E.H., 1998. The gas permeability of clay-bearing fault gouge at 20°C. In: Jones, G., et al. (Eds.), Faulting, Fault Sealing and Fluid Flow in Hydrocarbon Reservoirs, pp. 147–156. Geological Society Special Publication 147.
Fisher, Q.J., Knipe, R.J., 2001. The permeability of faults within siliciclastic petroleum reservoirs of the North Sea and Norwegian continental shelf. Mar. Petrol. Geol. 18, 1063–1081.
Flodin, E.A., Aydin, A., Durlofsky, L.J., Yeten, B., 2001. Representation of fault zone permeability in reservoir flow models. In: Society of Petroleum Engineers Annual Technical Conference and Exhibition, New Orleans.
Fossen, H., Schultz, R.A., Shipton, Z.K., Mair, K., 2007. Deformation bands in sandstone: a review. J. Geol. Soc. Lond. 164, 755–769.
Glennie, K.W., 1983. Early Permian (Rotliegendes) palaeowinds of the North Sea area. Sediment. Geol. 34, 245–265.
Glennie, K.W., Buller, A.T., 1983. The Permian Weissliegend of NW Europe: the partial deformation of aeolian dune sands caused by the Zechstein transgression. Sediment. Geol. 35, 43–81.
Healy, D., 2012. Anisotropic poroelasticity and the response of faulted rock to changes in pore-fluid pressure. Geol. Soc. Lond. 367, 201–214. Special Publications.
Kang, D.H., Yun, T.S., Lau, Y.M., Wang, Y.H., 2012. DEM simulation on soil creep and associated evolution of pore characteristics. Comput. Geotech. 39, 98–106.
Klinkenberg, L.J., 1941. The permeability of porous media to liquids and gases. Am. Pet. Inst. Drill. Prod. Pract., 200–213.
Lewis, J.J.,M., 1988. Outcrop-derived quantitative models of permeability heterogeneity for genetically different sand bodies. In: SPE Annual Technical Conference and Exhibition, 2–5 October 1988, Houston, Texas.
Li, X., Li, X., 2009. Micro-macro quantification of the internal structure of granular materials. J. Eng. Mech. 135 (7), 641–656.
Mauldon, M., Rohrbaugh, M.B., Dunne, W.M., Lawdermilk, W., 1999. Fracture Intensity Estimates Using Circular Scanlines. American Rock Mechanics Association, 99, 0777, conference paper.
Meyer, R., 2002. Anisotropy of sandstone permeability. CREWES Res. Rep. 14.
Peacock, J.D., Berridge, N.G., Harris, A.L., May, F., 1968. Geology of the Elgin District. In: Memoirs of the Geological Survey. H.M.S.O, Scotland, pp. 54–77.
Prieto, M., 2010. Quantification of the Changes in Reservoir Quality Around Fault Zones. Unpublished MSc thesis. University of Aberdeen.
Quinn, O.F., 2005. Fault Controlled Fluid Flow and Quartz Cementation in Porous Sandstones. Unpublished PhD thesis. University of Edinburgh.
Saillet, E., Wibberley, C.A.J., 2010. Evolution of cataclastic faulting in high-porosity sandstone, Basin du Sud-Est, Provence, France. J. Struct. Geol. 32, 1590–1608.
Saillet, E., Wibberley, C.A.J., 2013. Permeability and flow impact of faults and deformation bands in high-porosity sand reservoirs: Southeast Basin, France, analog. AAPG Bull. 97 (3), 437–464.
Schneider, C.A., Rasband, W.S., Eliceiri, K.W., 2012. NIH image to imagej: 25 years of image analysis. Nat. Methods 9, 671–675.
Shipton, Z.K., Evans, J.P., Robeson, K.R., Forster, C.B., Snelgrove, S., 2002. Structural heterogeneity and permeability in faulted eolian sandstone: implications for subsurface modeling of faults. AAPG Bull. 86 (5), 863–883.
Shotton, F.W., 1956. Some aspects of the New Red sandstone desert in Britain. Liverp. Manch. Geol. J. 1, 450–465.
Sibson, R.H., 2000. Fluid involvement in normal faulting. J. Geodyn. 29, 469–499.
Tanikawa, W., Shimamoto, T., 2009. Comparison of Klinkenberg-corrected gas permeability and water permeability in sedimentary rocks. Int. J. Rock Mech. Min. Sci. 46, 229–238.
Torabi, A., Fossen, H., 2009. Spatial variation of microstructure and petrophysical properties along deformation bands in reservoir sandstones. AAPG Bull. 93, 919–938.
Underhill, J.R., 1991. Implications of Mesozoic-recent basin development in the western Inner Moray Firth, UK. Mar. Petrol. Geol. 8, 359–369.
Vermilye, J.M., Scholz, C.H., 1998. The process zone: a microstructural view of fault growth. J. Geophys. Res. 103, 12,123–12,237.
Wibberley, C.A.J., Shimamoto, T., 2003. Internal structure and permeability of major strike-slip fault zones: the median tectonic line in Mie prefecture, Southwest Japan. J. Struct. Geol. 25, 59–78.

Wibberley, C.A.J., Shimamoto, T., 2005. Earthquake slip weakening and asperities explained by thermal pressurization. Nature 7051, 689–692.
Zhang, S., Tullis, T.E., 1998. The effect of fault slip on permeability and permeability anisotropy in an artificial quartz gouge. Tectonophysics 295, 41–52.
Zhu, W., Montési, L.G.J., Wong, T.F., 2002. Effects of Stress on the Anisotropic Development of Permeability during Mechanical Compaction of Porous Sandstones. Geological Society, London, pp. 119–136. Special Publications 200.
Zoback, M.D., Byerlee, J.D., 1976. Effect of high-pressure deformation on permeability of Ottawa sand. Bull. Am. Assoc. Petrol. Geol. 60, 1531–1542.